Sensors and Actuators B 137 (2009) 48–55

Contents lists available at ScienceDirect

Sensors and Actuators B: Chemical

journal homepage: www.elsevier.com/locate/snb

Inducing analytical orthogonality in tungsten oxide-based microsensors using materials structure and dynamic temperature control

K.D. Benkstein[a,*], B. Raman[a,b], D.L. Lahr[a], J.E. Bonevich[c], S. Semancik[a]

[a] National Institute of Standards and Technology, Chemical Science and Technology Laboratory, 100 Bureau Drive, Gaithersburg, MD 20899, USA
[b] Laboratory of Cellular and Synaptic Neurophysiology, National Institute of Health (NICHD, NIH), 35 Convent Drive Room 3A106, MSC 3715, Bethesda, MD 20892-3715, USA
[c] National Institute of Standards and Technology, Materials Science and Engineering Laboratory, 100 Bureau Drive, Gaithersburg, MD 20899, USA

ARTICLE INFO

Article history:
Received 8 August 2008
Received in revised form 8 October 2008
Accepted 9 October 2008
Available online 5 November 2008

Keywords:
Chemiresistor
Microhotplate
Nanowire
Nanoparticle

ABSTRACT

The influence of material structure and dimension on the chemical sensing performance was investigated as a function of sensor operating temperature. Polycrystalline tungsten oxides (WO_3) were prepared both as nanowires of different diameters ($d \approx 100$ nm, 175 nm; $l = 4$–5 μm) using a template-directed electrodeposition process, and as a continuous film through thermal decomposition of peroxytungstate solution. The WO_3 materials were integrated with microscale conductometric platforms featuring millisecond dynamic temperature control up to 500 °C. The nanowires and film were assessed for efficacy as transducers in gas-phase chemical sensors using these platforms, both in a fixed-temperature operating mode and in a dynamic pulsed-temperature operating mode. Statistical analysis of the tungsten oxide chemiresistor responses to analytes at varied operating temperatures revealed that orthogonal information can be obtained from stoichiometrically similar materials; the differences were exaggerated by probing the sensor responses with different dynamic temperature programs. We conclude that nanowire sensors yield non-redundant analytical information with respect to their complementary film-based sensor. These results demonstrate that as sensors move to nanoscale structures, unique interactions will differentiate the materials and the devices' performance from their microscale counterparts.

Published by Elsevier B.V.

1. Introduction

How do the size, dimension and morphology of a sensing material impact its performance? Metal- and metal-oxide-based nanostructures have been attracting significant interest in chemical sensing applications [1–9] owing to the small size and related characteristics (e.g., surface area, surface-to-volume ratios, quantum confinement). Of particular interest to us is the emerging role of nanomaterials as the active chemiresistor in chemical sensing applications [8–17]. Preliminary results do suggest that there are benefits to be gained by employing these nanostructured sensing materials in terms of response speed and sensitivity, which may be attributed to an increased diffusion rate of analytes through the sensing materials and their large surface-to-bulk ratio, respectively [5–9]. However, whether the differences in scale and structure of sensing materials create only similar sensors with improvements in their response speed and sensitivity, or result in quasi-unique sensors capable of generating orthogonal analytical information about a chemical species is not clear [7,8]. One-dimensional nanomaterials have been recently applied as the active sensing material in chemical sensors as reported by several groups for various sensor configurations [4–6,17–19]. For sensing applications, the nanoparticulate structure is also attractive, as it increases the number of grain boundaries in the active material where sensing interactions are believed to occur [20].

Here we describe a method to determine whether sensing material morphology imparts the potential for analytical orthogonality by probing the responses of three tungsten oxide chemiresistors differing in directed structure and dimensions. As a sensor material, tungsten oxide (WO_3) nanomaterials are receiving a significant amount of attention [21–26]. We have prepared two chemical sensors with active materials based upon polycrystalline nanowires of different diameters, and one sensor with a polycrystalline film. We determine that the three structures, while possessing similar surface chemistry and nanoparticulate building blocks, can provide analytically different transient responses based upon their thermal operating history and the selected target analyte.

* Corresponding author.
E-mail address: kurt.benkstein@nist.gov (K.D. Benkstein).

0925-4005/$ – see front matter. Published by Elsevier B.V.
doi:10.1016/j.snb.2008.10.029

2. Experimental

2.1. Tungsten(VI) oxide materials preparation

Polycrystalline tungsten oxide nanowires were made via template-directed electrodeposition followed by calcination. Briefly, one side of a track-etched polycarbonate filtration membrane (d_{pore} = 50 nm or 100 nm, l_{mem} = 6 μm) was coated by thermal evaporation with a silver film to serve as a working electrode. The WO_3 nanowires were deposited at constant potential (−0.5 V vs. Ag/AgCl) in the template from a peroxytungstate solution (Supplemental Fig. 1) [27]. Nanowires were isolated by first dissolving the Ag working electrode in 25% nitric acid, followed by dissolution of the template in chloroform. The nanowires were collected by centrifugation, and washed with chloroform and 2-propanol several times. After each wash, the nanowires were collected by centrifugation and then redispersed by sonication. The nanowires were finally dispersed in 2-propanol. Thin films of WO_3 were prepared via thermal decomposition of the peroxytungstate solution [28] to make comparisons between nanowire-based active sensing materials and film-based materials. To determine the effect of sintering on nanowire morphology, an aliquot of nanowire dispersion was allowed to dry in a small glass tube that was subsequently heated in a furnace to 480 °C in air for 1 h. The sintered nanowires were then dispersed in 2-propanol and deposited onto a TEM (transmission electron microscopy) grid for analysis. The WO_3 materials were characterized by optical, scanning electron and transmission electron microscopies. X-ray photoelectron spectra (XPS) were measured using monochromatic Al K (alpha) radiation. A Shirley background was applied to the W 4f spectra, which were then fit using Voigt profiles. All spectra were referenced to the surface oxide of the aluminum substrate at 74.4 eV.

2.2. Sensor preparation and evaluation

The WO_3 materials were deposited onto three individual microhotplate sensor platforms in a multi-element array that facilitates conductometric measurements with control of sensor operating temperatures [11,29,30]. The microhotplate platforms are 100 μm platforms suspended over a pit etched into the substrate silicon. A poly-silicon heater, embedded in the microhotplate platform, provides temperature control for materials processing or conductometric (chemiresistive) sensor operation. Electrical contact for simple resistive measurements is made to the sensing material (film or nanowires) via interdigitated platinum electrodes, which cover the surface of the microhotplate. The digits are nominally 2 μm wide with 2 μm gaps. All materials were deposited from freshly sonicated dispersions in 2-propanol (nanowires) or water:2-propanol solution (peroxytungstate solution) using a microcapillary pipette (id_{cap} = 75 μm). After the solvent dried, the sensing materials were calcined to 480 °C in flowing zero-grade dry air for 1 h. Sensor testing was carried out using a computer-controlled, automated gas-flow and data-collection system. Analytes were delivered in zero-grade dry air from gas cylinders.

The sensor response levels were calculated as $(G_{gas} - G_{air})/G_{air}$, where G_{gas} is the conductance of the sensor in the presence of an analyte, and G_{air} is the conductance of the analyte in the background condition of dry air. The response times were calculated as the time for the conductance to change from 10% to 90% of the total conductance change ($G_{gas} - G_{air}$). All analyses of TPS data were done using custom programs in a commercial software package. Conductance measurements of different materials at fifteen ramp and fifteen base temperatures were concatenated to form a multi-dimensional sensor response that was used for all analysis.

To analyze the similarity/orthogonality of responses of any two WO_3 morphologies (M_1, M_2) at two operating temperatures (T_1, T_2), we used Pearson's correlation coefficients. If $g(M_1, T_1)$ is a one-dimensional vector of conductance response of M_1 at temperature T_1 to any of the test analytes (CH_3OH or CO) during different trials, and $g(M_2, T_2)$ a one-dimensional vector of conductance measurements made using M_2 at temperature T_2, then the correlation between responses of M_1 at T_1 and M_2 at T_2 is calculated as

$$\frac{n\sum g(M_1,T_1)g(M_2,T_2) - \sum g(M_1,T_1)\sum g(M_2,T_2)}{\left(\left(n\sum g(M_1,T_1)^2 - \left(\sum g(M_1,T_1)\right)^2\right)\left(n\sum g(M_2,T_2)^2 - \left(\sum g(M_2,T_2)\right)^2\right)\right)^{1/2}}$$

where n in the number of trials. Only the absolute values of the correlation coefficients with significance $p < 0.05$ (t-test) are shown.

For visualizing the sensor response, we used principal component analysis (PCA), which is a linear dimensionality reduction technique [31]. In PCA, the six-dimensional sensor array responses (1 ramp and 1 base temperature per sensing element; three elements) were projected onto the first two or three dimensions, defined by the first few eigenvectors (with largest eigenvalues) of the response covariance matrix that captures most of the variance in the dataset.

3. Results and discussion

For our studies, polycrystalline nanowires composed of WO_3 were prepared by the adaptation of a literature electrochemical deposition method [27] to template-directed synthetic methodology [32,33]. As deposited, the nanowires are largely amorphous as demonstrated by TEM studies (Fig. 1a). However, nanocrystals of WO_3 with diameters of 10–15 nm were also observed in the as-deposited nanowires, and were surrounded by amorphous material. After calcining the WO_3 nanowires at 480 °C in air for 1 h and examining again by TEM, it was apparent that the wires had completely converted to crystalline material, while retaining the nanocrystalline size of 10–15 nm (Fig. 1b–e). The nanowires themselves, then, are built of nanocrystals with many grain boundaries along and within the length of the wire. To provide a dramatically different assembly of nanoparticles for comparison with the nanowire materials, WO_3 films were prepared by the thermal decomposition of a microdrop of the peroxytungstate solution [28]. The chemical states of the tungsten oxide materials were probed by XPS (Fig. 2). Tungsten is identified from a survey scan from the 4s, 4p 1/2, 4p 3/2, 4d 5/2 and 4f 7/2 peaks at 596.4 eV, 493.9 eV, 425.4 eV, 244.5 eV and 35.4 eV, respectively. High-energy-resolution region scans (Fig. 2, inset) for both the nanowires and the film were well fit by Voigt profiles, indicating that a single chemical species is present at the surface for both the film and the nanowires, each having an energy of 35.5 eV for the W 4f 7/2 peak, in good agreement with previous reports for tungsten(VI) oxide [34].

Further characterization of the materials was conducted after the WO_3 nanowires were isolated from their template and then integrated with temperature-controlled microsensor platforms ("microhotplates," see Section 2 for more information about the National Institute of Standards and Technology (NIST) microsensor technology) via microcapillary pipette [35]. The microhotplate platform also provides a convenient method for calcining the materials. Fig. 3 shows SEM (scanning electron microscopy) micrographs of (a) a microhotplate and various tungsten oxide sensor materials (b and c; see also Supplemental Fig. 2) nanowires prepared in a 100 nm pore-diameter template deposited on a microhotplate, and subsequently calcined at 480 °C in dry air and (d) a nanostructured film prepared by thermal decomposition of a peroxytungstate precursor. As deposited from the dispersion, the nanowires sparsely cover

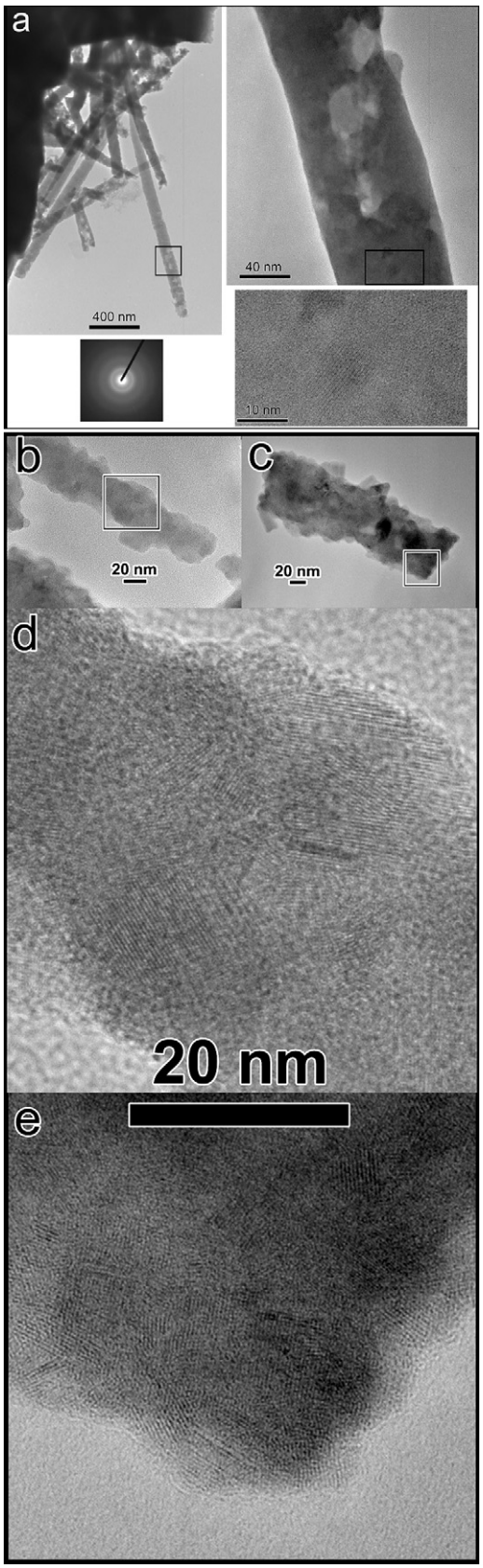

Fig. 1. TEM micrographs of WO_3 nanowires (a) as prepared, and (b–e) after calcination in air at 480 °C. The high-magnification micrographs (d and e) correspond with the boxes in the lower magnification images (b and c, respectively).

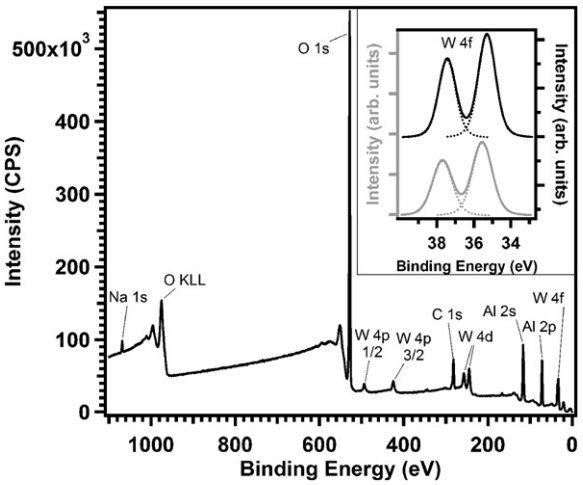

Fig. 2. XPS analyses of the tungsten oxide materials. Shown in the main plot is a survey scan of the nanowires on an aluminum substrate. The inset shows the W 4f peaks of nanowires (bottom, gray) and a film (top, black). The dotted lines are Voigt fits of the data.

the microhotplate and tend to form clusters, as shown in Fig. 3b. However, individual, isolated nanowires are also present in significant numbers, e.g., as shown in Fig. 3c. The length of the nanowires is controlled by the time of the deposition, and ultimately restricted by the thickness of the template. In the case of the nanowires used here, the deposition time was 180 min, which results in nanowires of ≈4 μm in length, appropriate for bridging the gaps between the interdigitated electrodes on the microsensor devices. Although the nominal pore diameter of the template is 100 nm, the thickness of the wires tends to be larger, with a diameter of ≈125 nm near the tips and a diameter of ≈175 nm toward the middle of the nanowire length. The same trend is observed for the nanowires deposited in the 50 nm pore-diameter templates: nanowires on average are ≈60 nm near the tips and ≈100 nm in the middle. The tapering effect is due to the non-cylindrical pores present in the track-etched polycarbonate membranes [32]. EDS analyses (not shown) confirm the XPS analyses that the nanowires are W-based materials, and that the silver electrode used for electrodeposition has been successfully removed. The film has continuous coverage over the space of the interdigitated contacts and shows nanoscale structure.

A comparison of sensor efficacy was made between the three WO_3 nanoparticle materials: nanowires of different diameters (50 nm and 100 nm pores: "nw50" and "nw100", respectively) and a film. To establish the viability of these WO_3 nanowires as conductometric sensors, in comparison with the film, we first examined their performance at a single operating temperature. Fig. 4 shows the responses at 375 °C (fixed-temperature sensing, FTS) of three sensors based upon the three different structural building blocks. As expected the baseline conductances for the nanowire materials are much lower than for the film, owing to the significantly lower coverage of the nanowires (estimated at several hundred nanowires on a 100 μm × 100 μm platform from SEM imaging) over the interdigitated contacts. The FTS study does, however, demonstrate the efficacy of the nanowire materials as chemical sensors (see Table 1 for an example of CH_3OH FTS results). Despite the small amount of active material, the nw50 sensor demonstrates good signal-to-noise (S/N ≈ 32 for 2 μmol/mol methanol). The generally good sensitivity and S/N ratio of the nw50 sensor may be attributed to the enhanced surface roughness of the calcined WO_3 nanowires, as shown in the TEM studies (Fig. 1). The nanocrystalline domains also offer many active sensing sites at the grain boundaries, which may contribute to the generally strong sensor

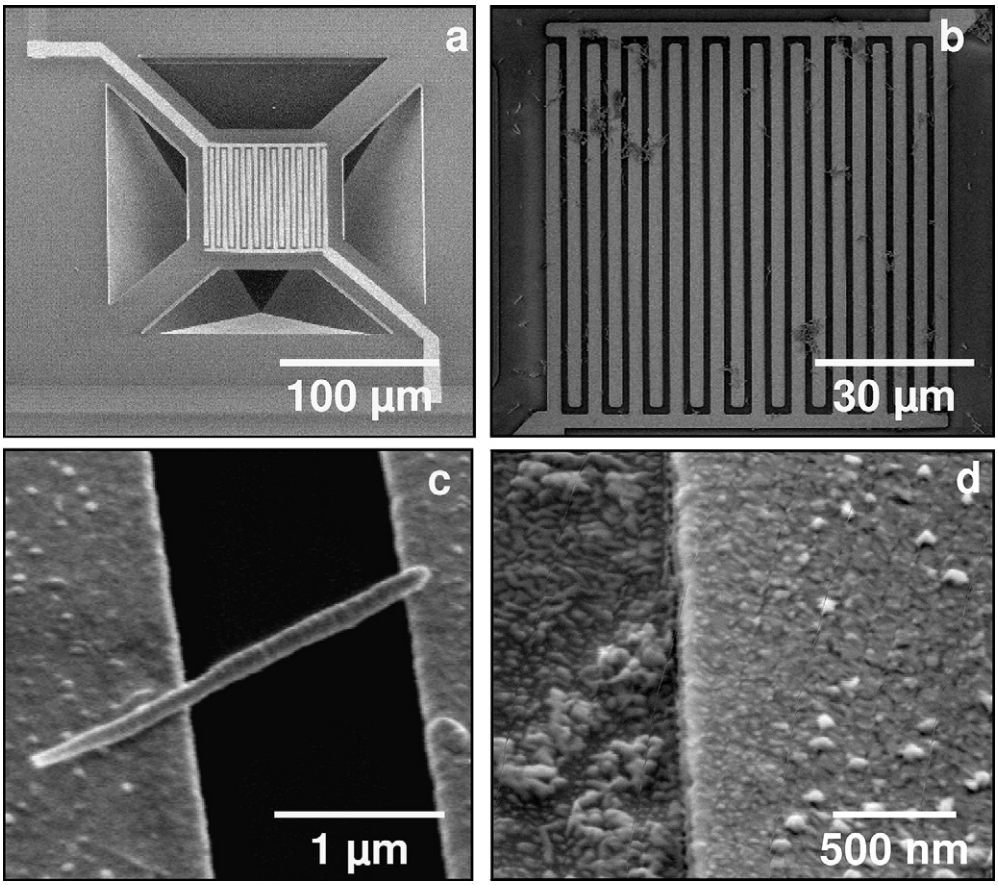

Fig. 3. SEM micrographs of (a) a clean microhotplate (b) a microhotplate sparsely covered with WO_3 nanowires (c) an isolated WO_3 nanowire across two contacts on a microhotplate, and (d) a WO_3 film on a microhotplate produced via the thermal decomposition of a peroxytungstate precursor.

response [20,36]. Notably, the response times are quicker for the nw50 sensor versus the film-based sensor by a factor of ≈2. The relatively quick response time of the nanowire sensor is attributed to the readily accessible surface of the materials with respect to a comparatively dense film sensor [8].

From the FTS experiments, there are no readily apparent distinguishing features between the responses of the three structures.

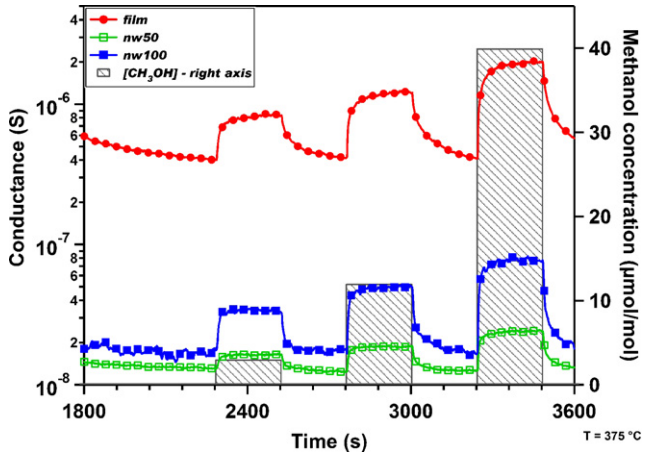

Fig. 4. The responses of WO_3 materials at a fixed temperature of 375 °C to presentations of methanol with an emphasis on differences in WO_3 morphology: thin film (red, filled circles); WO_3 nanowires, nw50 (green, open squares); WO_3 nanowires, nw100 (blue, filled squares). (For interpretation of the references to color in this figure legend, the reader is referred to the web version of the article.)

However, because of the small thermal time constant of the microhotplate platforms, it is possible (and beneficial) to rapidly change the temperature to sample a large temperature range yielding a high data density per unit time [30]. Fig. 5 shows the dynamic temperature program used to collect the responses of sensors. The base temperature between two pulsed-temperature measurements is always 140 °C. Measurements are made both at the end of the ramp temperature pulses (ramp measurements) and at the end of the base temperature pulses (base measurements). The baseline temperature between two temperature pulses allows "relaxation" (including chemically and thermally induced charge carriers) toward some base state prior to each ramp pulse. We then applied a general method to evaluate the differences in the complex and analytically rich sensor data in order to compare and contrast more thoroughly the responses from the three structurally different sensors to analytes and to operating temperature.

Shown in Fig. 6a are the averaged responses of the sensors to the presence of the three analytes using the temperature program of Fig. 5 (FTS and TPS data vs. time plots are shown in Supplemental Fig. 2). The three analytes are easily separable based on the conductometric measurements made using the three WO_3 sensors (Fig. 6a). The sensors were also exposed to varied concentrations of the three analytes (Supplemental Fig. 4a). However, the three concentrations are distinguishable only in the case of CH_3OH. Notice that for the three WO_3 sensors, the conductance decreases as the operating temperature increases from 60 °C to 210 °C for all three analytes, and then subsequently increases as the ramp temperature increases from 210 °C to 480 °C. Also, we note that the ramp and the base measurements are qualitatively similar to each other (Supplemental Fig. 4).

Table 1
Response strengths and times (±standard deviation of four trials) of WO_3 microsensors for varied concentrations of methanol in 1 slm dry air and with a sensor operating temperature of 425 °C.

[Methanol] (μmol/mol)	Response strength ($\Delta G/G_0$)		Response time (s)	
	Nanowire sensor (nw50)	Film sensor	Nanowire sensor (nw50)	Film sensor
2	0.41 ± 0.05	1.9 ± 0.1	51 ± 19	88 ± 3
4	0.58 ± 0.08	3.0 ± 0.1	36 ± 10	86 ± 3
8	0.86 ± 0.04	4.9 ± 0.3	47 ± 8	109 ± 5
16	1.28 ± 0.09	8.3 ± 0.5	61 ± 9	120 ± 5
20	1.52 ± 0.04	9.8 ± 0.5	60 ± 24	122 ± 5

In order to determine the effect of thermal history on the sensor response, the sensors were operated with a temperature program that covered the same range (ramp temperature varied from 60 °C to 480 °C, base temperature held at 140 °C), but with 1 °C temperature steps for the ramp (421 total ramp temperatures, rather than 15). For clarity, and for direct comparison with the larger temperature increments, only the data corresponding to the 15 ramp temperatures of the TPS program shown in Fig. 5 are used. Only the highest concentration of CH_3OH (red) and CO (green) were used in this study. The mean sensor responses to the two analytes are shown in Fig. 6b. It can be clearly seen that unlike the previous case with 30 °C increments (Fig. 6a), here the conductance is almost monotonic with temperature. There is only a decrease in conductance from 60 °C to ≈100 °C, showing that the thermal history does have an effect on raw sensor operations.

To visualize the high-dimensional sensor response obtained by concatenating the base and ramp temperature responses of the three WO_3 sensors, we use principal component analysis (see Section 2). Fig. 6c shows the six-dimensional sensor array response for the data in Fig. 6a (1 ramp and 1 base measurement per temperature step per sensing element; three elements) after linear projection along the first three principal components (accounts for 97.41% variance in the data) [31]. A similar plot (Fig. 6d) shows the six-dimensional sensor array response for 421 ramp temperatures after linear projection along the first two principal components (accounts for 93.64% variance in the data) for the data in Fig. 6b. It can be seen that for the 30 °C temperature steps, the identity of the analyte introduces variance along one direction (color: CH_3OH, red; NO_2, blue; CO, green), that the analyte concentration causes additional variance within the analyte cluster (shading from dark to light), and that the temperature introduces variance along a different direction (arrows indicating sensor temperature from low to high). Furthermore, the separability between the analytes varies with the operating temperature (Fig. 6a), suggesting the importance of thermal history in sensor responses. Thus, by choosing an appropriate temperature program, we may be able to enhance differences in the responses of the three sensors here.

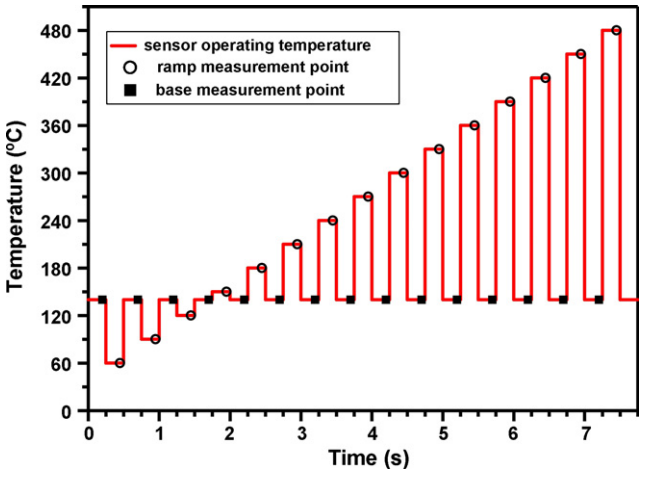

Fig. 5. The temperature program used to obtain TPS data with 30 °C increments between ramp steps. Conductance measurements are made at each open circle (ramp) and filled square (base).

We assessed the orthogonality/similarity between the three WO_3 sensors' conductometric transient responses at the fifteen different temperature steps with 30 °C increments. For this purpose, we used a measure based upon correlation coefficients (see Section 2) to compare the information content of the transients as a function of both material morphology and the analyte targeted: the greater the correlation, the more related or redundant is the information available. Fig. 7a shows a color-coded representation of the correlation coefficients for the ramp data across all the three morphologies at various temperatures for air samples (background) and the three analytes studied (Supplemental Fig. 4a shows the correlation coefficients for the base-temperature data). Each pixel shows the absolute value of significant correlation ($p < 0.05$) between responses of a WO_3 morphology at one temperature (T_1) to each condition (background or analyte) versus its response at a second temperature (T_2). Only the highest concentrations of the analytes were included for this analysis. The red pixels indicate higher correlations and the blue pixels represent lower correlations. Diagonal blocks provide self-correlation patterns and off-diagonal blocks present cross-correlation across WO_3-material morphologies.

It can be observed from Fig. 7a that, in the case of the air samples, the low-temperature and high-temperature transients create separate correlation bands. Interestingly, for some conditions these bands are conserved across different WO_3 morphologies, while for others, the bands are different. For CH_3OH, for example, the responses of the three WO_3 sensors are highly correlated at each of the fifteen different temperatures. Cross-correlations (off-diagonal blocks) between the sensing materials also reveal high degrees of correlation, indicating that the three morphologically different WO_3 sensors generate only redundant information about CH_3OH. However, in the cases of NO_2 and CO, the correlation between the transients of the three WO_3 sensors decreases suggesting generation of non-redundant information. We note that the correlation between transients of the nanowire-based sensors is high for NO_2, while between the film and either of the nanowire sensors the correlation is much lower. That is, the nanowire-based sensors provide similar information with respect to each other, but non-redundant with respect to the film-based sensor for NO_2 using this temperature program. These results clearly show that dissimilar analytical information is obtained from these nanowire WO_3 sensors by cycling through temperatures for certain chemical species. To further corroborate our findings and to show that these correlation patterns across the WO_3 sensors are truly a function of the analyte present and not the age of the sensors, we repeated this analysis for air samples collected on three different days (Supplemental Fig. 5b).

The capability to perform rapid temperature changes during sensor operation enables elucidation of the differences between

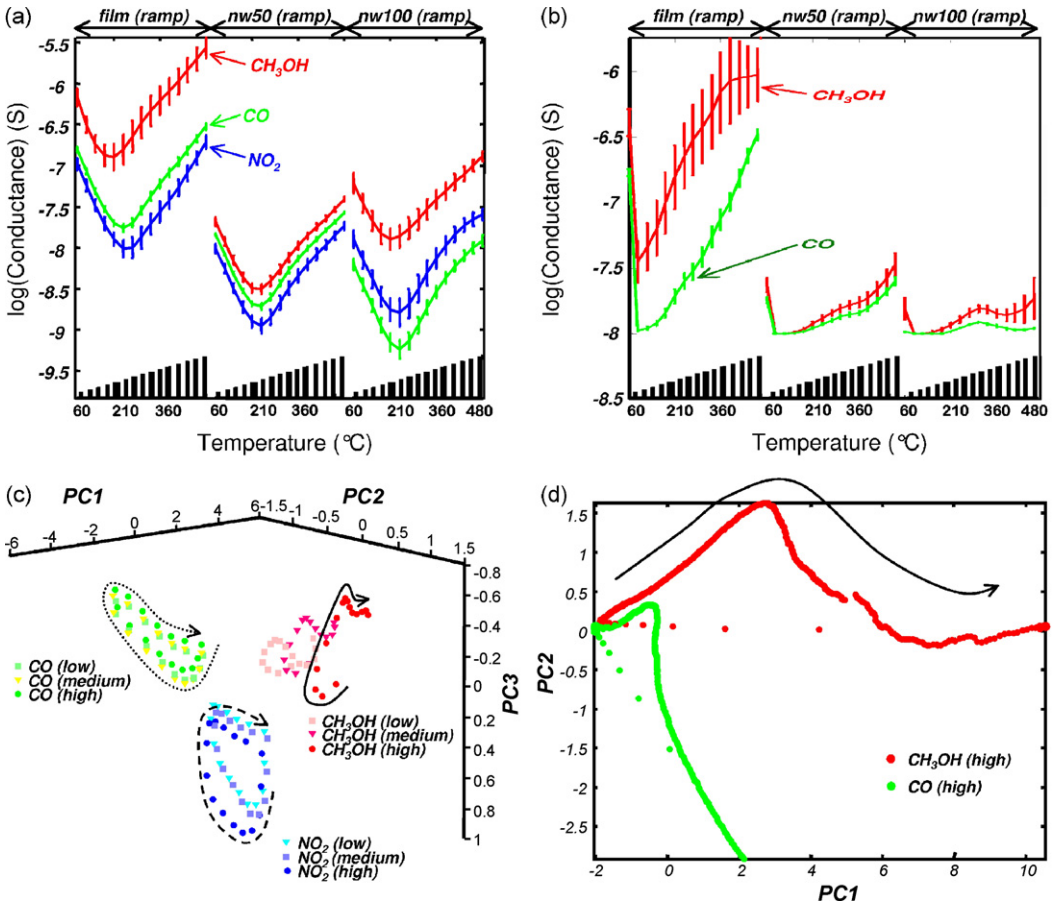

Fig. 6. Results from the statistical analysis of the conductometric measurements made using a temperature program with 30 °C increments (a and c) and 1 °C increments (b and d). (a) Mean ramp measurements of the three different WO_3 sensors to three analytes: methanol (CH_3OH; dark red—40 μmol/mol), carbon monoxide (CO; dark green—200 μmol/mol), and nitrogen dioxide (NO_2; dark blue—1 μmol/mol). The error bars represent the standard deviations. (b) Mean ramp measurements of the three different WO_3 sensors to the highest concentration of methanol and carbon monoxide at the 15 ramp temperatures shown in Fig. 5 (other ramp-temperature data not shown for clarity). (c) Projection of the six-dimensional sensor response for the data shown in Fig. 6a, with varied analyte concentrations included, (one ramp and one base measurement per temperature step per sensor type; three sensor elements) along the first three principal components (*variance captured* = 97.12%), color-coded by the chemical identity. The arrows show the trend with increasing ramp temperature (the different patterning is to aid in tracing their paths). (d) Projection of the six-dimensional sensor response for the data shown in Fig. 6b (one ramp and one base measurement per temperature per sensor type; three sensor elements) along the first two principal components (*variance captured* = 93.64%), color-coded by the chemical identity. The arrows show the trend with increasing ramp temperature. (For interpretation of the references to color in this figure legend, the reader is referred to the web version of the article.)

their responses. This is shown by the banding patterns in Fig. 7 for the correlation between the film and nanowire sensors (most apparent for NO_2). While the film produces similar information regardless of the sensor temperature, the nanowire-based sensors (with respect to the film) are yielding non-redundant information of varied degrees at the low-range, mid-range and high-range temperatures, primarily due to different thermal transients from these sensor-material morphologies. These results are in agreement with the expectation that different physical phenomena tend to occur at different temperatures ranges (adsorption at low temperatures, desorption and reaction at higher temperatures).

For the WO_3 sensors, we observed that, as a function of ramp temperature, the sensor conductance initially decreases with increasing temperature, and then increases with higher temperature steps. However, the inflection point is different for the different temperature-step increments: for the smaller step size ($\Delta T = 1\,^{\circ}C$), the inflection point is at ≈100 °C, while for the larger step size ($\Delta T = 30\,^{\circ}C$), the inflection point is at 210 °C. To further study the effect of thermal history on the sensor response we compared the transients for these two temperature steps as shown in Fig. 7b. We found that the temperature step size had little effect on the transient response to background air. However, in the case of CH_3OH and CO, differences in temperature-step size produced dissimilar transient responses in both the nanowire sensors. Interestingly, the differences observed between the transient CO responses for the morphologically different WO_3 sensors for larger temperature steps were not observed for the smaller step size. Together with the temperature banding in the correlation plots, these results suggest that by designing a temperature program that probes a range of interactions between the sensor and its environment, and by altering the thermal history of the sensor, non-redundant, analytically rich information can be extracted from a nanostructured metal-oxide chemiresistor. Furthermore, subtle differences in sensor performance may be enhanced, as shown by the low correlation between nanowire- and film-based sensors for the detection of NO_2.

We note that as a result of the structural differences, the three sensors will have different mass loads on the microhotplates, especially with respect to the film versus the nanowires, which can contribute to the differences in their performance. We expect that the films, which completely cover the microhotplates, to respond somewhat less quickly to changes in operating temperature than do the nanowire-based sensors (relatively small amount of material on the microhotplate). This may be supported by the relative

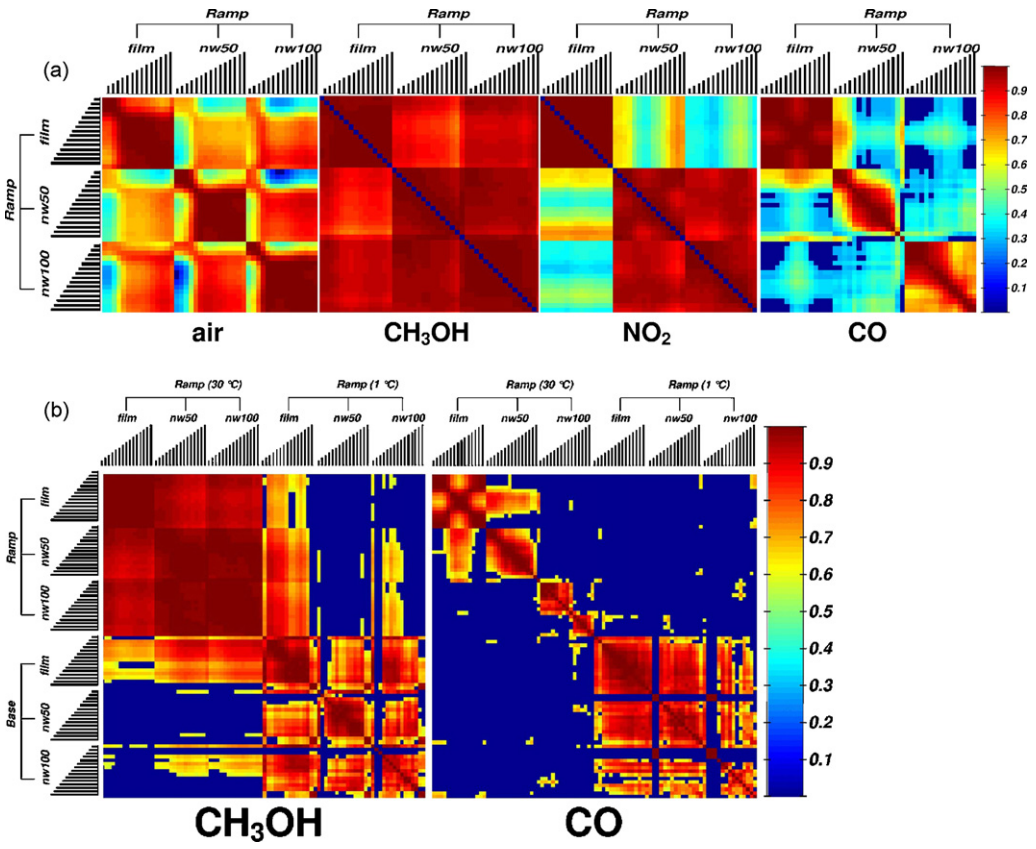

Fig. 7. Results from the statistical analysis of the conductometric measurements made using temperature programs (60 °C to 480 °C) with 30 °C and 1 °C increments. (a) Correlation coefficients ($p < 0.05$) between the three WO_3 sensors' responses at the 15 ramp-temperature measurements using 30 °C increments as shown in Fig. 5 for air (background), CH_3OH, NO_2 and CO. (b) Comparison of correlation coefficients ($p < 0.05$) between the three WO_3 sensors responses' at the 15 ramp temperatures corresponding to the ramp temperatures in Fig. 5 with 30 °C and 1 °C increments (other temperature data not included in the analysis).

response times of the film versus the nanowire-based sensor, which suggest that the film responds more slowly to changes in its environment. We also note that the varied responses may be attributed to differences in the ratios between bulk and surface structures (i.e., the nanowires are almost exclusively surface material, while the film will have substantial bulk material that does not interact with analyte gas) [18]. Furthermore, the particles that form the basis of nanowires may also be changing with increasing time at the highest temperatures of the temperature program (Supplemental Fig. 2), although we do not believe that this greatly impacts the results of this study, based upon the similar correlation patterns for each of the air backgrounds in the three experiments (Supplemental Fig. 5). The similar correlation patterns indicate that the sensors are not fundamentally changing during the lifetime of our studies. The differences between the sensors is enhanced and clearly shown by use of the dynamic temperature control.

Ultimately, the different responses to the analytes for the three sensors do not come from induced differences in materials stoichiometry or surface composition (all are tungsten(VI) oxide after thermal processing in air as shown by XPS); rather, it is the result of induced changes in sensor material structure from film to nanowires of different diameter. We have shown that these differences can be exaggerated by probing their responses using temperature programs that sample a range of temperatures with larger steps. That is, dynamic temperature control provides a means of probing the role of nanoscale structure and dimension in chemical sensor operation. While we did not examine sensor reproducibility in this study (expected to be low because of the uncontrolled orientation and number of nanowires), we also note that this technique has the potential to reveal subtle differences in film performance for nominally identical sensors, thus providing a tool for assessing the reproducibility of mass-produced sensors. More generally, these results demonstrate the influence of material structure on sensing properties and that morphological manipulation produces sensors of different capabilities.

Acknowledgments

We acknowledge the technical assistance of C. B. Montgomery in preparing the microhotplate sensor platforms. We also thank Professor T. E. Mallouk, R. M. Hernandez and Y. Cao, and Professor K. J. Stevenson for useful discussions on nanowire and WO_3 electrodeposition. BR was supported by a NIH-NIST Joint Postdoctoral Associateship Award and DLL was supported by a NIST Postdoctoral Associateship Award, both administered through the National Research Council.

Appendix A. Supplementary data

Supplementary data associated with this article can be found, in the online version, at doi:10.1016/j.snb.2008.10.029.

References

[1] K. Sivakumar, B. Panchapakesan, Electric field-assisted deposition of nanowires on carbon nanotubes for nanoelectronics and sensor applications, J. Nanosci. Nanotechnol. 5 (2005) 313–318.
[2] Q. Wan, Q.H. Li, Y.J. Chen, T.H. Wang, X.L. He, J.P. Li, C.L. Lin, Fabrication and ethanol sensing characteristics of ZnO nanowire gas sensors, Appl. Phys. Lett. 84 (2004) 3654–3656.

[3] X.T. Zhou, J.Q. Hu, C.P. Li, D.D.D. Ma, C.S. Lee, S.T. Lee, Silicon nanowires as chemical sensors, Chem. Phys. Lett. 369 (2003) 220–224.
[4] M.C. McAlpine, H. Ahmad, D.W. Wang, J.R. Heath, Highly ordered nanowire arrays on plastic substrates for ultrasensitive flexible chemical sensors, Nat. Mater. 6 (2007) 379–384.
[5] X.J. Huang, Y.K. Choi, Chemical sensors based on nanostructured materials, Sens. Actuators B 122 (2007) 659–671.
[6] E. Comini, Metal oxide nano-crystals for gas sensing, Anal. Chim. Acta 568 (2006) 28–40.
[7] M.E. Franke, T.J. Koplin, U. Simon, Metal and metal oxide nanoparticles in chemiresistors: does the nanoscale matter? Small 2 (2006) 36–50.
[8] V.V. Sysoev, J. Goschnick, T. Schneider, E. Strelcov, A. Kolmakov, A gradient microarray electronic nose based on percolating SnO_2 nanowire sensing elements, Nano Lett. 7 (2007) 3182–3188.
[9] C.S. Moon, H.R. Kim, G. Auchterlonie, J. Drennan, J.H. Lee, Highly sensitive and fast responding CO sensor using SnO_2 nanosheets, Sens. Actuators B-Chem. 131 (2008) 556–564.
[10] K.D. Benkstein, C.J. Martinez, G. Li, D.C. Meier, C.B. Montgomery, S. Semancik, Integration of nanostructured materials with MEMS microhotplate platforms to enhance chemical sensor performance, J. Nanoparticle Res. 8 (2006) 809–822.
[11] K.D. Benkstein, S. Semancik, Mesoporous nanoparticle TiO_2 thin films for conductometric gas sensing on microhotplate platforms, Sens. B Actuators 113 (2006) 445–453.
[12] C.J. Martinez, B. Hockey, C.B. Montgomery, S. Semancik, Porous tin oxide nanostructured microspheres for sensor applications, Langmuir 21 (2005) 7937–7944.
[13] B. Deb, S. Desai, G.U. Sumanasekera, M.K. Sunkara, Gas sensing behaviour of mat-like networked tungsten oxide nanowire thin films, Nanotechnology 18 (2007).
[14] C.L. Dai, M.C. Liu, F.S. Chen, C.C. Wu, M.W. Chang, A nanowire WO_3 humidity sensor integrated with micro-heater and inverting amplifier circuit on chip manufactured using CMOS–MEMS technique, Sens. B Actuators 123 (2007) 896–901.
[15] F. Hernandez-Ramirez, A. Tarancon, O. Casals, J. Arbiol, A. Romano-Rodriguez, J.R. Morante, High response and stability in CO and humidity measures using a single SnO_2 nanowire, Sens. B Actuators 121 (2007) 3–17.
[16] E. Comini, C. Baratto, G. Faglia, M. Ferroni, G. Sberveglieri, Single crystal ZnO nanowires as optical and conductometric chemical sensor, J. Phys. D: Appl. Phys. 40 (2007) 7255–7259.
[17] D.C. Meier, S. Semancik, B. Button, E. Strelcov, A. Kolmakov, Coupling nanowire chemiresistors with MEMS microhotplate gas sensing platforms, Appl. Phys. Lett. 91 (2007).
[18] A. Kolmakov, M. Moskovits, Chemical sensing and catalysis by one-dimensional metal-oxide nanostructures, Ann. Rev. Mater. Res. 34 (2004) 151–180.
[19] S.J. Pearton, D.P. Norton, F. Ren, The promise and perils of wide-bandgap semiconductor nanowires for sensing, electronic, and photonic applications, Small 3 (2007) 1144–1150.
[20] N. Barsan, U. Weimar, Conduction model of metal oxide gas sensors, J. Electroceram. 7 (2002) 143–167.
[21] T. Maekawa, J. Tamaki, N. Miura, N. Yamazoe, Gold-loaded tungsten-oxide sensor for detection of ammonia in air, Chem. Lett. (1992) 639–642.
[22] J. Tamaki, Y. Okochi, S. Konishi, Effect of oxide-electrode interface on dilute NO_2 sensing properties of WO_3 thin film nanosensors, Electrochemistry 74 (2006) 159–162.
[23] J. Tamaki, Z. Zhang, K. Fujimori, M. Akiyama, T. Harada, N. Miura, N. Yamazoe, Grain-size effects in tungsten oxide-based sensor for nitrogen-oxides, J. Electrochem. Soc. 141 (1994) 2207–2210.
[24] J. Tamaki, Nano-design of oxide particles and electrode structure for high sensitivity NO_2 sensor using WO_3 thick film, Mater. Res. Soc. Symp. Proc. 828 (2005) A1.4.1–A1.4.11.
[25] G.A. Wang, Y.A. Ji, X.R. Huang, X.Q. Yang, P.I. Gouma, M. Dudley, Fabrication and characterization of polycrystalline WO_3 nanofibers and their application for ammonia sensing, J. Phys. Chem. B 110 (2006) 23777–23782.
[26] K.M. Sawicka, A.K. Prasad, P.I. Gouma, Metal oxide nanowires for use in chemical sensing applications, Sensor Lett. 3 (2005) 31–35.
[27] E.A. Meulenkamp, Mechanism of WO_3 electrodeposition from peroxytungstate solution, J. Electrochem. Soc. 144 (1997) 1664–1671.
[28] K. Yamanaka, H. Oakamoto, H. Kidou, T. Kudo, Peroxotungstic acid coated films for electrochromic display devices, Jpn. J. Appl. Phys. 25 (1986) 1420–1426.
[29] S. Semancik, R.E. Cavicchi, M. Gaitan, J.S. Suehle. Temperature-controlled micromachined arrays for chemical sensor fabrication and operation, U.S. Patent 5,345,213, September 6, 1994.
[30] S. Semancik, R.E. Cavicchi, Kinetically controlled chemical sensing using micromachined structures, Acc. Chem. Res. 31 (1998) 279–287.
[31] R. Duda, P.E. Hart, D.G. Stork, Pattern Classification, second ed., Wiley-Interscience, NY, New York, 2000.
[32] C. Schönenberger, B.M.I. van der Zande, L.G.J. Fokkink, M. Henny, C. Schmid, M. Krüger, A. Bachtold, R. Huber, H. Birk, U. Staufer, Template synthesis of nanowires in porous polycarbonate membranes: electrochemistry and morphology, J. Phys. Chem. B 101 (1997) 5497–5505.
[33] M.L. Tian, J.U. Wang, J. Kurtz, T.E. Mallouk, M.H.W. Chan, Electrochemical growth of single-crystal metal nanowires via a two-dimensional nucleation and growth mechanism, Nano Lett. 3 (2003) 919–923.
[34] R.J. Colton, J.W. Rabalais, Electronic-structure of tungsten and some of its borides, carbides, nitrides, and oxides by X-ray electron-spectroscopy, Inorg. Chem. 15 (1976) 236–238.
[35] G. Li, C. Martinez, S. Semancik, J.A. Smith, M. Josowicz, J. Janata, Effect of morphology on the response of polyaniline-based conductometric gas sensors: nanofibers *vs.* thin films, Electrochem. Solid-State Lett. 7 (2004) H44–H47.
[36] B. Panchapakesan, D.L. DeVoe, M.R. Widmaier, R. Cavicchi, S. Semancik, Nanoparticle engineering and control of tin oxide microstructures for chemical microsensor applications, Nanotechnology 12 (2001) 336–349.

Biographies

Kurt D. Benkstein earned his B.S. degree in Chemistry in 1995 from Iowa State University, and his M.S. and Ph.D. degrees in Chemistry from Northwestern University in 1996 and 2000, respectively. He went to the National Renewable Energy Laboratory in 2000 as a postdoctoral researcher to study the relation between film morphology and electron transport in dye-sensitized nanoparticle solar cells. In 2003, he joined the National Institute of Standards and Technology as a Research Chemist to examine nanostructured materials as conductometric gas sensors.

Baranidharan Raman received the B.S. degree in computer science with distinction from the University of Madras, Madras, India, in 2000 and the M.S. and Ph.D. degrees in computer science from Texas A&M University, College Station, in 2003 and 2005, respectively. He is currently an NIH/NIST joint Postdoctoral Fellow in the Laboratory of Cellular and Synaptic Neurophysiology (NICHD), and the Process Sensing Group (NIST), National Institute of Standards and Technology, Gaithersburg, MD. His research interests include combining computational and electrophysiological approaches to study neural computations especially olfactory signal processing, sensor-based machine olfaction, machine learning, intelligent systems and robotics, human–computer interaction, and dynamical systems.

David L. Lahr received his B.S. in Chemistry from the University of Rochester in 1998, and his Ph.D. in Physical Chemistry from the Massachusetts Institute of Technology in 2006. His research interests include surface science of catalysts, semiconductors and sensors. He is currently an Analyst Programmer at Tessella, Inc.

John E. Bonevich received a B.S.E in Metallurgical Engineering from the University of Michigan (1986) and a Ph.D. in Materials Science and Engineering from Northwestern University (1991). He joined the Materials Science and Engineering Laboratory at NIST in 1995. He is the Director of the MSEL Microscopy Facility. Research interests include structure–property relationships in microelectronic interconnects, magnetic multilayer thin films, ferroelectric and optical materials, and nanostructured materials.

Steve Semancik is the Project Leader of the Chemical Microsensor Program at the National Institute of Standards and Technology (NIST) in Gaithersburg, Maryland. He received his B.S. degree in physics from Rensselaer Polytechnic Institute and his M.Sc. and Ph.D. degrees, also in physics, from Brown University. Dr. Semancik's professional research career began as a National Research Council Postdoctoral Fellow, and has been centered in the fields of surface science and sensor science. His recent work has focused on developing improved nanomaterials for chemical and biochemical sensing, and combining such high performance materials with micromachined platforms to realize advanced microsensor devices and operating modes. Dr. Semancik is an elected Fellow of both the American Physical Society and American Vacuum Society. He has served as a Member of the Editorial Board of two sensor journals, and is a Member of the Steering Committee of the International Meeting on Chemical Sensors. He has authored or coauthored 131 papers (including five reviews), one book chapter, and five patents. Dr. Semancik has been the recipient of a number of awards, including the Chemical Science and Technology Laboratory Technical Achievement Award at NIST, and the U.S. Department of Commerce Silver and Bronze Medals.